Journal of Molecular Structure 1241 (2021) 130685

Contents lists available at ScienceDirect

Journal of Molecular Structure

journal homepage: www.elsevier.com/locate/molstr

Exploration of structural, electronic and third order nonlinear optical properties of crystalline chalcone systems: Monoarylidene and unsymmetrical diarylidene cycloalkanones

Akbar Ali[a,1], Muhammad Khalid[b,1,*], Zia Ud Din[c,*], Hafiz Muhammad Asif[d,*], Muhammad Imran[e], Muhammad Nawaz Tahir[f], Muhammad Ashfaq[f], Edson Rodrigues-Filho[c]

[a] Department of Chemistry, Government College University Faisalabad, Pakistan
[b] Department of Chemistry, Khwaja Fareed University of Engineering and Information Technology, Rahim Yar Khan 64200, Pakistan
[c] LaBioMMi, Departamento de Química, Universidade Federal de São Carlos, CP 676, São Carlos, SP 13.565-905, Brazil
[d] Institute of Chemical Sciences, Bahauddin Zakariya University, Multan 60800, Pakistan
[e] Department of Chemistry, Faculty of Science, King Khalid University, P.O. Box 9004, Abha 61413, Saudi Arabia
[f] Department of Physics, University of Sargodha, Sargodha, Pakistan

ARTICLE INFO

Article history:
Received 14 February 2021
Revised 23 April 2021
Accepted 10 May 2021
Available online 18 May 2021

Keywords:
Arylidene Cycloalkanones
SC-XRD
DFT Study
NLO

ABSTRACT

In the current study monoarylidene and unsymmetrical diarylidene cycloalkanes, **MBMHP, MABP, MBHP**, and **MBCP** have been prepared. Their molecular structures were confirmed by SC-XRD. Accompanying the experimental studies, quantum chemical investigation is performed at the M06/6-311+G(d,p) level, with the natural bond orbital analysis (NBO) performed at the ωB97XD/6-311+G(d,p) level. NBO study showed that the hyper-conjugation and intermolecular charge transfer play a remarkable role in stabilizing the crystals and also endorsed the SC-XRD investigations. Furthermore, the band gap of orbitals explained the chemical reactivity and charge transfer phenomena in the above-mentioned crystals. The smallest HOMO/LUMO band gap (4.127 *eV*) is exhibited by **MABP** molecule while the highest gap value is found for **MBHP** to be 4.768 *eV*.. Global reactivity parameters (GRP) are also explored from the energies of HOMO/LUMO. Among all crystals **MBHP** has higher value of hardness (η = 2.384 *eV*) while **MABP** showed higher global softness (σ = 0.242307 *eV*). So, from GRP it is revealed that all the studied crystals are less reactive but more stable as suggested by NBO and SC-XRD investigations. NLO study showed that the crystal **MBMHP** has the higher value of linear polarizability$<\alpha>$ and second hyperpolarizability $<\gamma>$ 216.36 and 1.06 $\times$ 10^4 *a.u* respectively, among all the synthesized crystals. NLO properties of these synthesized crystals may play a significant contribution for the NLO technological applications.

Introduction

Monoarylidene and unsymmetrical diarylidene alkanones are pharmaceutically active compounds [1]. Synthetic bis(arylidene)s are well known for their cytotoxic capability against human ovarian tumor cell line A2780-CP70 that is found resistant towards the famous cisplatin [2]. Moreover, monoarylidene and unsymmetrical diarylidene alkanones derivatives have also been found to have anti-inflammatory [3] antibacterial [4], antimicrobial [5], anti-tubercular [6],antimalarial [7], antifungal [8], antioxidant [9], anti-viral [10], antimitotic [11], anti-tubulin [12], antitumor [13], anti-fertility [14], anti-parasitic [15], anticancer [16], and neuroprotective [17] capabilities. Both symmetrical and unsymmetrical curcuminoids have shown their medicinal importance [18]. Together with their medicinal importance, these diarylidene cycloalkanone derivatives have been studied for their photophysical properties along with their electron donor-acceptor ability and found to have potential applications in the two-photon absorption (TPA) processes [19]. In recent time, the nonlinear optical (NLO) properties exploration has attracted significant attention of the scientific community (both theoretical and experimental researchers) as materials with strong NLO properties have found momentous applications in various fields of science and technology [20], especially the areas of nuclear science, medicine, biophysics, solid physics, chemical dynamics, surface-interface and materials science

* Corresponding authors.
E-mail addresses: khalid@iq.usp.br (M. Khalid), zia.ufscar@gmail.com (Z.U. Din), hmasifc@gmail.com (H.M. Asif).
[1] These authors contributed equally to this work.

https://doi.org/10.1016/j.molstruc.2021.130685
0022-2860/

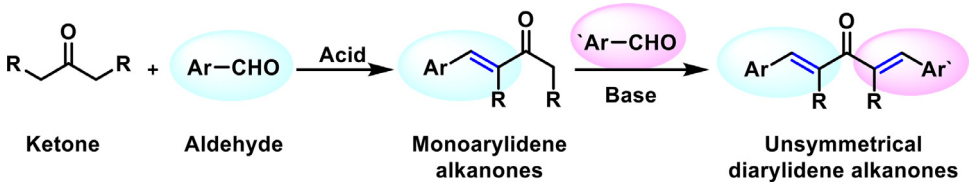

Scheme 1. Synthesis and structural features of monoarylidene and unsymmetrical diarylidene alkanones compounds

are worth mentioning[21]. It is important to mention that organic materials are capable of strong NLO behavior and have significant advantages over the inorganic counterparts due to their ease of solution process ability, low cost, flexibility for device fabrications and low toxic nature [22]. There are various classes of organic compounds that show significant NLO responses. Among these organic compounds conjugated molecules, perylenes, phosphonate compounds, fullerenes, polymers, thiophenes and organic dyes are important to mention [23]. Arylidene alkanones (both monoarylidene and unsymmetrical diarylidene alkanones) are also a significant class of organic compounds that have been investigated for the NLO properties [24]. Density functional theory (a computational modelling approach) is extensively used for the exploration of nonlinear optical ability of organic materials. Here, we present our investigation related to the synthesis of monoarylidene and unsymmetrical diarylidene cycloalkanones (Scheme 1), their complete structural verification by single-crystal analysis along with their nonlinear optical exploration via detailed DFT calculations.

Experimental Section

Chemistry

Chemicals utilized in this research work were bought from renowned standard companies like Acros Chemicals and Sigma-Aldrich and were used as received. In order to observe the reaction speed TLC plates (pre-coated silica gel G-25-UV254) were used. The NMR studies (1H and13C) were performed using the Brüker AVANCE 400 at 400 MHz and 100 MHz, respectively, where the tetramethyl silane (TMS) was used as internal reference.

General Procedure

Preparation of compounds 1 and 2

Cyclopentanone and aldehyde (*o*-methyl benzaldehyde in case of compound 1 and *p*-nitro benzaldehyde in case of compound 2) were taken in a ratio of 1:1, in a two necked (50 mL) round bottom flask. Through this reaction mixture, HCl gas was passed till it turns red colored. Stirring was continued for 8 h. The reaction mixture was washed with $NaHSO_3$ solution after diluting with toluene. After separating the organic layer it was dried over anhydrous Na_2SO_4 and the solvent was removed by rotary evaporation. The purified product was obtained via vacuum distillation to yield the compounds 1 and 2 and recrystallization was performed using ethanol (See Scheme 2).

Preparation of compound 3

The compound 3 was synthesized following the above procedure for the synthesis of compounds 1 and 2. Accordingly, tetrahydro-*4H*-pyran-4-one and *o,m*-dimethoxy benzaldehyde were taken in a two-necked round-bottom flask (50 mL) in 1:1 ratio followed by passing of the HCl gas through the reaction mixture and waited for the reaction mixture to turns red colored. The reaction mixture was stirred for 8 h before diluting it with toluene and then was washed with a solution of $NaHSO_3$. After the workup, the separated organic layer was dried over anhydrous Na_2SO_4. Finally, the purified product was obtained using vacuum distillation yielding compound 3 that was recrystallized using ethanol (See Scheme 2).

Preparation of compound 4

To a stirred solution of compound 3 and p-methoxy benzaldehyde in ethanol (5 mL) at room temperature, the NaOH solution in ethanol (4 mL, 50 mol) was added and stirring was continued. After completion (observed by TLC), the solvent of the reaction mixture was evaporated by rotary evaporator. The reaction mixture was diluted in ethyl acetate and then the extraction was performed with $NaHSO_3$ solution. The organic layer was dried over anhydrous Na_2SO_4. Upon concentrating using rotary evaporator, the crude product was recovered as yellow precipitate that was purified using column chromatography. Upon recrystallization using ethanol, pure crystals of compound 4 were recovered and used for the SC-XRD analysis (See Scheme 2).

Characterization of compounds

(1). (E)-2-(2-methylbenzylidene)cyclopentanone (MBMHP)

The spectroscopic data of the title compound was found to be in total correspondence to the reports in literature [25]. ^{1}H NMR (400 MHz, $CDCl_3$) δ 7.59 (t, J = 2.7 Hz, 1H), 7.42 (dd, J = 7.4, 1.9 Hz, 1H), 7.29 – 7.17 (m, 3H), 2.90 (td, J = 7.2, 2.7 Hz, 2H), 2.51 – 2.34 (m, 5H), 2.01 (p, J = 7.5 Hz, 2H); ^{13}C NMR (100 MHz, $CDCl_3$) δ 207.9, 138.9, 136.8, 134.3, 130.5, 129.8, 129.2, 128.6, 125.8, 38.0, 29.4, 20.5, 20.0.

(2). ((E)-2-(4-(dimethylamino)benzylidene)cyclopentanone (MABP)

The spectroscopic data of the title compound was found in total correspondence to the reported literature[26]. ^{1}H NMR (400 MHz, $CDCl_3$) δ 7.46 (d, J = 8.9 Hz, 2H), 7.34 (t, J = 2.6 Hz, 1H), 6.75 (d, J = 8.1 Hz, 2H), 3.02 (s, 6H), 2.94 (td, J = 7.2, 2.5 Hz, 2H), 2.36 (t, J = 8.0 Hz, 2H), 2.00 (p, J = 7.6 Hz, 2H); ^{13}C NMR (100 MHz, $CDCl_3$) δ 208.1, 150.6, 133.2, 132.5, 131.4,112.2, 111.0, 40.4, 37.8, 29.4, 20.2.

(3). (E)-3-(2,3-dimethoxybenzylidene)dihydro-2H-pyran-4(3H)-one (MBHP)

The spectroscopic data of the title compound was found in total correspondence to the reported literature[26]. ^{1}H NMR (400 MHz, $CDCl_3$) δ 7.73 (s, 1H), 6.98 (t, J = 8.0 Hz, 1H), 6.89 (dd, J = 8.2, 1.4 Hz, 1H), 6.60 (dd, J = 7.8, 1.1 Hz, 1H), 4.64 (d, J = 2.1 Hz, 2H), 3.99 (t, J = 6.1 Hz, 2H), 3.80 (s, 3H), 3.74 (s, 3H), 2.61 (t, J = 6.1 Hz, 2H); ^{13}C NMR (100 MHz, $CDCl_3$) δ 196.2, 152.8, 148.5, 134.2, 131.2, 128.5, 123.7, 122.0, 113.8, 68.7, 65.6, 61.1, 55.8, 39.9.

(4). 3-((E)-2,3-dimethoxybenzylidene)-5-((E)-4-methoxybenzylidene)tetrahydro-4H-pyran-4-one (MBCP)

^{1}H NMR (400 MHz, $CDCl_3$) δ 8.03 (d, J = 1.8 Hz, 1H), 7.82 (d, J = 5.6 Hz, 1H), 7.32 (dd, J = 8.6, 3.8 Hz, 2H), 7.10 (dd, J = 10.6, 5.3

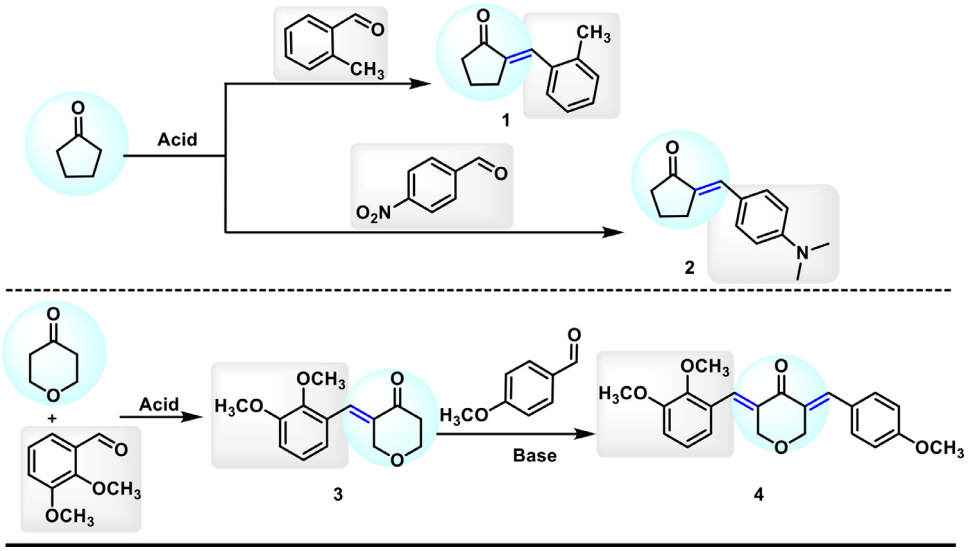

Scheme 2. Synthetic route for the accomplishment of the organic crystalline compounds:**1(MBMHP), 2 (MABP), 3 (MBHP),** and **4 (MBCP)**.

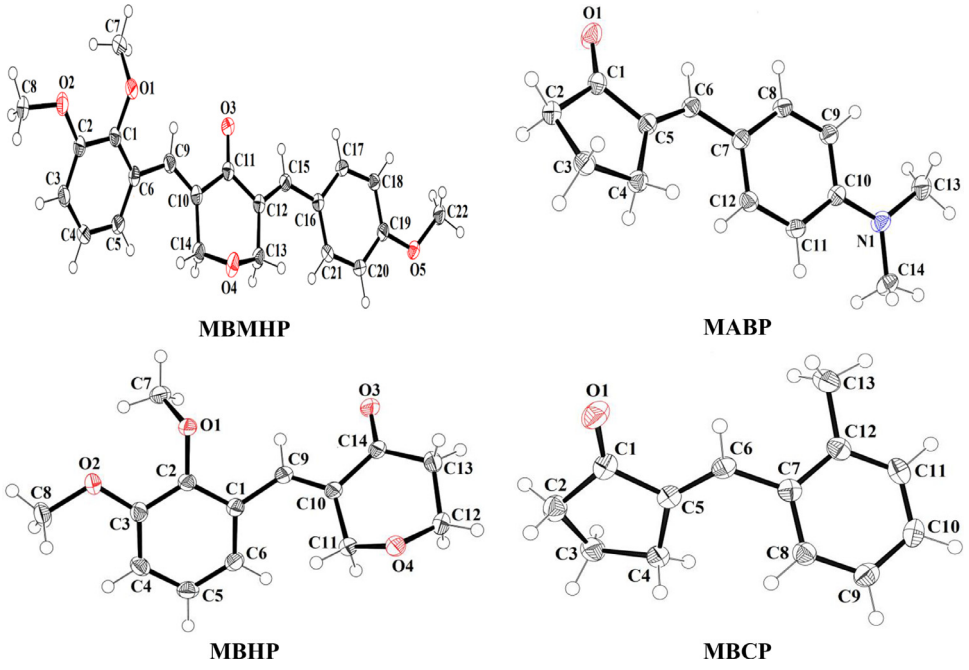

Fig. 1. ORTEP illustration of **MBMHP, MABP, MBHP** and **MBCP** drawn at 50% probability level. H-atoms are shown by tiny rings of arbitrary radii.

Hz, 1H), 7.00 – 6.95 (m, 3H), 6.73 (dt, J = 11.2, 5.6 Hz, 1H), 4.96 (d, J = 1.8 Hz, 2H), 4.79 (t, J = 5.3 Hz, 2H), 3.93 – 3.90 (m, 3H), 3.88 (s, 3H), 3.83 (s, 3H).^{13}C NMR (100 MHz, CDCl3) δ 185.5, 160.6, 153.0, 148.4, 136.5, 134.1, 132.6, 131.6, 131.2, 129.2, 127.6, 123.8, 122.2, 114.3, 113.5, 69.0, 68.7, 61.4, 55.9, 55.4.

In the **MBMHP** (Fig. 1, Table 1), the tetrahydro-2*H*-pyran ring A (C10-C14/O4) is not planar but the basal plane B (C10-C14/O3) is planar with r.m.s (root mean square) deviation of 0.0387 Å. The ring O-atom is out of basal plane B and deviated at the distance of -0.6833 (2) Å from the basal plane B. Ring Puckering inspection manifests that the tetrahydro-2H-pyran ring A has puckering amplitude Q=0.5235(12) Å with θ=124.20(14)° and φ=167.58(18)°. The part of aldehyde group named as 3-methylbenzene-1,2-diol group C (C1-C6/C9/O1/O2) is found to be planar with r.m.s deviation of 0.0235 Å. The terminal carbon atoms (C7/C8) of methoxy groups are at the distance of 1.1686 (2) and 0.2678 (2) Å, respectively, from the plane of group C. The 1-methoxy-4-methylbenzene group D is unevenly planar with root mean square (r.m.s) deviation of 0.0675 Å. The dihedral angle of basal plane B with group C and D is 39.25 (4)° and 11.5 (7)°, respectively, whereas the dihedral angle between C/D is 31.12 (4)°. The C-H···O bonding is responsible for the intermolecular linkage. The molecules are interlinked in the form of dimers to form $R_2^1(7)$ loop by two types of C-H···O bonding, where O-atom is from carbonyl oxygen attached to tetrahydro-2H-pyran ring A. In first type of C-H···O bonding, CH is from the ring part of anisole moiety (C16-C22/O5) while in second type of C-H···O bonding, CH is from the terminal methyl moiety of the anisole part. These dimers are interlinked by C18-H18…O3 and C18-H18-O4 bonding as revealed in Fig. 2 and specified in Table 2. The O-atom of anisole moiety and O-atom directly attached with carbon atom (C7) are not engaged in hydrogen bonding. Moreover, the presence of C-H···π interaction gives further stability in the crystal packing. One of the ring CH of group C of a molecule located at asymmetric position is interacted with the

Table 1
Experimental data of the title compounds.

MBMHP		**MABP**	**MBHP**	**MBCP**
CCDC	2017959	2017960	2017961	2017962
Chemical formula	$C_{22}H_{22}O_5$	$C_{14}H_{17}NO$	$C_{14}H_{16}O_4$	$C_{13}H_{14}O$
M_r	366.39	215.28	248.27	186.24
Crystal system, space group	Monoclinic, $P2_1/c$	Monoclinic, $P2_1/c$	Monoclinic, $P2_1/n$	Orthorhombic, *Aba*2
Temperature (K)	150(2)	150(2)	150(2)	150(2)
a, b, *c* (Å)	11.309 (3), 8.779 (2), 18.800 (4)	13.372 (2), 7.4908 (11), 12.2915 (18)	4.0235 (1), 13.9297 (5), 21.7483 (7)	14.7638 (7), 19.9779 (10), 6.9582 (3)
α, β, γ (°)	90, 101.987 (5), 90	90, 111.436 (3), 90	90, 93.573 (1), 90	90, 90, 90
V (Å^3)	1825.8 (8)	1146.0 (3)	1216.54 (7)	2052.32 (17)
Z	4	4	4	8
Density (Mg/m3)	1.333	1.248	1.356	1.206
F(000)	776	464	528	800
Radiation type	Mo $K\alpha$	Mo $K\alpha$	Cu $K\alpha$	Cu $K\alpha$
Wavelength (λ)	0.71073 Å	0.71073 Å	1.54178 Å	1.54178 Å
μ (mm^{-1})	0.094	00.078	0.817	0.578
Crystal size (mm)	0.45 × 0.23 × 0.12	0.55 × 0.35 × 0.14	0.18 × 0.17 × 0.15	0.34 × 0.21 × 0.17
Data collection				
Diffractometer	Bruker APEXII CCD diffractometer	Bruker APEXII CCD diffractometer	Bruker APEXII CCD diffractometer	Bruker APEXII CCD diffractometer
Absorption correction	multi-scan (SADABS; Bruker, 2007)	multi-scan (SADABS; Bruker, 2007)	multi-scan (SADABS; Bruker, 2007)	multi-scan (SADABS; Bruker, 2007)
No. of measured, independent and observed [$I > 2\sigma(I)$] reflections	11440, 3872, 3225	12361, 2441, 2212	15676, 2144, 2000	6661, 1762, 1748
R_{int}	0.018	0.019	0.030	0.020
Theta range for data collection	1.841-26.730	1.636-26.743	3.770- 66.580	4.426-66.574
Index ranges	-14≤ h ≤14, -11≤ k ≤8, -23≤ l ≤ 22	-16≤ h ≤16, -9≤ k ≤9, -15≤ l ≤ 11	-4≤ h ≤4, -16≤ k ≤16, -25≤ l ≤ 25	-17≤ h ≤16, -23≤ k ≤23, -8≤ l ≤ 8
$(\sin\theta/\lambda)_{max}$ (Å^{-1})	0.633	0.633	0.595	0.595
Refinement				
$R[F^2 > 2\sigma(F^2)]$, $wR(F^2)$, S	0.035, 0.092, 1.03	0.037, 0.098, 1.03	0.032, 0.086, 1.07	0.028, 0.070, 1.08
No. of reflections	3872	2441	2144	1762
No. of parameters	247	147	165	129
No. of restraints	-	-	-	1
H-atom treatment	H-atom parameters constrained	H-atom parameters constrained	H-atom parameters constrained	H-atom parameters constrained
$\Delta\rho_{max}$, $\Delta\rho_{min}$ (e Å^{-3})	0.22, −0.20	0.22, −0.21	0.20, −0.19	0.14, −0.21

Table 2
Hydrogen-bond geometry (Å, º) for the title compounds.

	D—H…A	**D—H**	**H…A**	**D…A**	**D—H…A**
	C8—H8A···O3^{i}	0.98	2.31	3.2231 (18)	155
	C18—H18…O3^{ii}	0.95	2.53	3.2309 (17)	131
	C18—H18…O4^{iii}	0.95	2.54	3.2939 (16)	137
MBMHP	C20—H20…O2^{iv}	0.95	2.41	3.2945 (16)	156
	C22—H22A…O3^{ii}	0.98	2.59	3.4171 (19)	142
	C—H…*π*	**C—H**	**H… *π***	**C… *π***	**C—H… *π***
	C5—H5…Cg(3)^{iv}	0.95	2.91	3.5703(17)	47
	C13—H13A… Cg(3)^{v}	0.99	2.83	3.7043(17)	57
	D—H…A	**D—H**	**H…A**	**D…A**	**D—H…A**
	C14—H14B…O1^{vi}	0.98	2.56	3.5025(15)	162
	C8—H8…O1^{vii}	0.95	2.59	3.4943 (14)	160
	C4—H4B…O1^{viii}	0.99	2.57	3.5547 (15)	170
MABP	C3—H3A…O1^{ix}	0.99	2.47	3.4509 (14)	170
	C—H…*π*	**C—H**	**H… *π***	**C… *π***	**C—H… *π***
	C13—H13A…Cg(2)^{x}	0.98	3.00	3.8240(15)	67
	C14—H14A… Cg(2)^{xi}	0.98	2.77	3.6254(14)	58
	D—H…A	**D—H**	**H…A**	**D…A**	**D—H…A**
	C8—H8A…O4^{xii}	0.98	2.56	3.3009 (16)	133
	C12—H12A…O3^{xiii}	0.99	2.60	3.3429 (16)	132
MBHP	C5—H5…O3^{xiv}	0.95	2.59	3.4994 (16)	161
	C7—H7C…O1^{xiii}	0.98	2.37	3.3520 (16)	177
	D—H…A	**D—H**	**H…A**	**D…A**	**D—H…A**
	C2—H2B…O1^{xv}	0.99	2.56	3.303 (2)	131
	C10—H10…O1^{xvi}	0.95	2.56	3.484 (2)	166
MBCP	**C—H…*π***	**C—H**	**H… *π***	**C… *π***	**C—H… *π***
	C3—H3A…Cg(2)^{xvii}	0.99	2.80	3.696(2)	66
	C9—H9… Cg(2)^{xv}	0.95	2.99	3.7246(19)	45

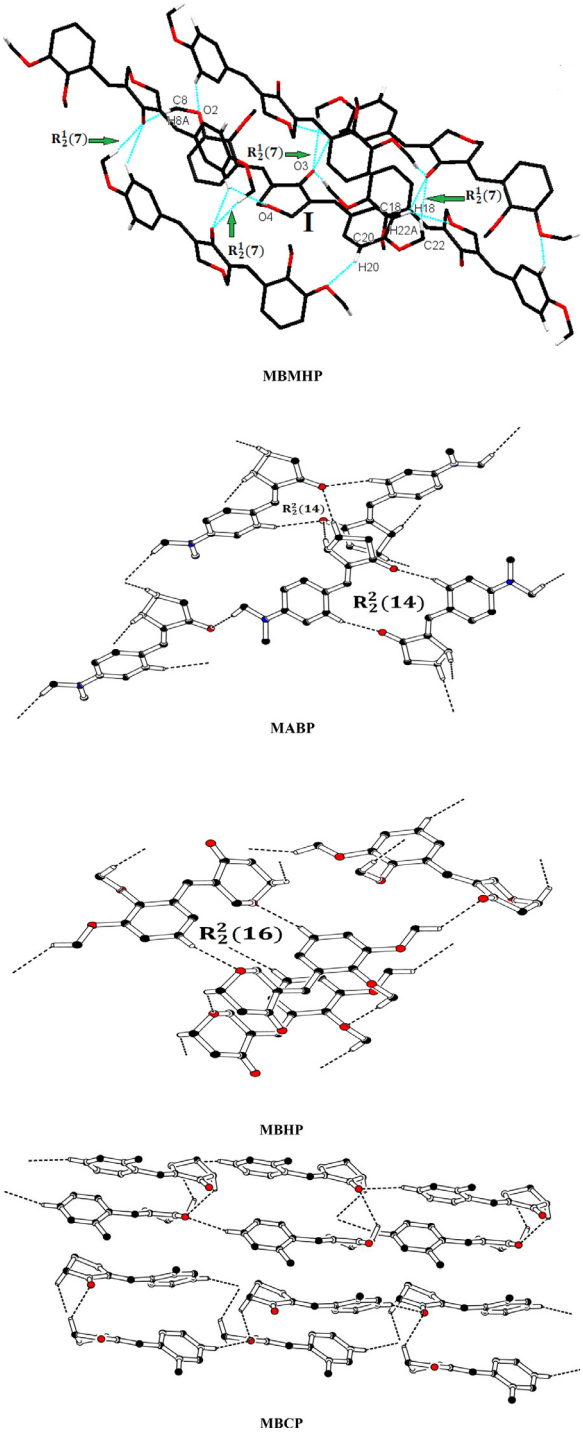

Fig. 2. Packing diagram of **MBMHP, MABP, MBHP** and **MBCP** showing dimerization of molecules through C–H...O bonding. H-atoms not engaged in hydrogen bonding are removed for clarity.

phenyl ring of anisole moiety of a molecule located at $-x$, $y-1/2$, $-z+1/2$ with H$\cdots\pi$ distance of 2.91 Å as shown Fig. S1 and given in Table 2. Similarly, One of the CH of the tetrahydro-2H-pyran ring A of a molecule located at asymmetric position is interacted with the phenyl ring of anisole moiety of a molecule located at $-x$, $-y$, $-z+1$ with H$\cdots\pi$ distance of 2.83 Å.

In the **MABP** (Fig. 1, Table 1), the cyclopentane ring A (C1-C5) is found to be not planar but the basal plane B (C1/C2/C4/C5/O1) is planar with r.m.s deviation of 0.0017 Å. The apical carbon atom (C3) is at the distance of 0.4287 (2) Å from basal plane B. Ring Puckering inspection manifests that the cyclopentane ring A has an envelope conformation on atom number C3. The N,N,4-trimethylaniline group C (C6-C14/N1) is planar with r.m.s deviation of 0.0281 Å and is oriented at the dihedral angle of 21.7 (4)° with respect to basal plane B. The molecules are interlinked in the form of dimers through C-H···O interaction to form $R_2^2(14)$ loop, where CH is from the aromatic six-membered ring as shown in Fig. 2 and given in Table 2. The two C-atoms (C3/C4) of cyclopentane ring A (for numbering see Fig. 1) are act as donor for O-atom of neighboring molecule also C14-H14B···O1 bonding is responsible for crystal packing. The presence of C-H$\cdots\pi$ interaction gives further assistances in strengthening of the crystal packing. CH of the dimethylamine moiety D of a molecule located at the asymmetric position is interacted with the phenyl ring of a molecule positioned at $-x$, $2-y$, $-z$ with H$\cdots\pi$ distance of 2.77 Å as shown in Fig. S1 and given in Table 2. Similarly, the other CH of the dimethylamine moiety D of a molecule located at asymmetric position is interacted with the phenyl ring situated at $-x$, $y+1/2$, $-z+1/2$ with H$\cdots\pi$ distance of 3.00 Å.

In the **MBHP** (Fig. 1, Table 1), the tetrahydro-2H-pyran ring A (C10-C14/O4) is not planar but the basal plane B (C10-C14) is found to be planar having r.m.s deviation of 0.0828 Å. The carbonyl O-atom is not in the plane B this time. The ring O-atom and carbonyl O-atom are deviated at the distance of 0.6451 (2) and -0.2642 Å, respectively from basal plane B. Ring Puckering inspection manifests that the tetrahydro-2H-pyran ring A has puckering amplitude Q = 0.5148(12) Å with θ = 42.22(14)° and φ=338.0(2)°. The part of aldehyde group named as 3-methylbenzene-1,2-diol group C (C1-C6/C9/O1/O2) is found to be planar with r.m.s deviation of 0.0188 Å. The terminal carbon atoms (C7/C8) of methoxy groups are at the distance of -1.2280 (2) and 0.1724 Å, respectively from plane of group C. The molecules are associated with each other in such a way to form dimers via C-H···O interaction to form $R_2^2(16)$ loop. Moreover, in this case CH is from the phenyl ring of 1,2-dimethoxybenzene while O-atom is from tetrahydro-2H-pyran ring E as shown in Fig. 2 and given in Table 2. The CH of ortho and meta-positioned methoxy group of 1,2-dimethoxybenzene moiety act as donor for O-atom of ortho-positioned methoxy group and carbonyl O-atom, respectively to connect molecules with each other. Similarly, CH of the tetrahydro-2H-pyran ring acts as donor for O-atom of same ring of another molecule to connect them. In this compound, the packing of molecules is further stabilized by the presence of cycle stacking interaction. The phenyl ring of molecule located at asymmetric positon interact with phenyl ring of a neighboring molecule located at $-x+1$, y, z with distance of 4.024 Å between the centroids as shown in Fig. S1.

In the **MBCP** (Fig. 1, Table 1), the cyclopentane ring A (C1–C5) is found to be not planar but the basal plane B (C1/C2/C4/C5/O1) is found to be planar having r.m.s deviation of 0.0072 Å. The apical carbon atom (C3) is at the distance of -0.4741 (3) Å from basal plane B. Ring Puckering inspection manifests that the cyclopentane ring A has an envelope conformation on atom number (C3). The toluene group C (C6–C13) is in plan having r.m.s deviation of 0.0199 Å oriented at the dihedral angle of 34.13 (6)° with respect to basal plane B. The molecules are interlinked through two types of C–H…O bonding. In first type of C–H…O bonding, CH is from phenyl ring whereas in second type of C–H…O bonding, CH is from cyclopentane ring as shown in Fig. 2 and given in Table 2. Molecules form infinite C14 chains through these C–H…O bonding along [100] crystallographic direction. Moreover, packing is further stabilized by the presence of C-H$\cdots\pi$ interaction. One of the CH of the cyclopentane ring A of a molecule located at asymmetric position is interacted with the phenyl ring of toluene group of a molecule located at $-x$, $-y+1/2$, z with H…π distance of 2.80 Å as

shown in Fig. S1 and given in Table 2. Similarly, One of the CH of the methyl group attached to phenyl ring of a molecule situated at asymmetric position is interacted with the phenyl ring of toluene group of a molecule positioned at $-x+3/2$, y, $z-1/2$ with H$\cdots\pi$ distance of 2.99 Å.

Symmetrycodes:(i) x, $-y+1/2$, $z-1/2$ (ii) $-x$, $-y+1$, $-z+1$ (iii) x, $-y+1/2$, $z+1/2$ (iv) $-x$, $y-1/2$, $-z+1/2$ (v) $-x$, $-y$, $-z+1$ (vi) $x-1$, $-y+3/2$, $z-1/2$ (vii) $-x+1$, $-y+2$, $-z+1$ (viii) $-x+1$, $y-1/2$, $-z+1/2$ (ix) x, $-y+3/2$, $z-1/2$ (x) $-x$, $y+1/2$, $-z+1/2$ (xi) $-x$, $2-y$, $-z$ (xii) $-x+3/2$, $y-1/2$, $-z+1/2$ (xiii) $x-1$, y, z; (xiv) $-x+1$, $-y$, $-z$; (xv) $-x+3/2$, y, $z-1/2$ (xvi) x, $y+1/2$, $z-1/2$ (xvii) $-x$, $-y+1/2$, z.

Computational details

With the assistance of Gaussian 09 program package [26], quantum chemical investigation of the title crystals has been performed. The primary structures of **MBMHP, MABP, MBHP** and **MBCP** have been obtained by the SC-XRD. The Density Functional Theory (DFT) [27–29] is study was performed at the M06/6-311+G(d,p) level [30]to obtain the optimized geometries. The M06 is more recently developed functional from Minnesota group of functionals as designed by Zhao and Truhlar [31,32]. It is the most advance functional of DFT and more considerably used now a days as an excellent agreement is found between experimental and DFT study at this level However, an infinitesimal difference is always foreseen for the reason that the experimental data correlate to the structures in solid phase, whereas DFT calculations are coupled to the gaseous phase. The absence of imaginary frequencies showed that the structures are successfully optimized. Furthermore, frontier molecular orbital analysis (FMOs) and nonlinear optical analysis (NLO) investigations were performed at the aforesaid level by using the optimized geometries of the title compounds. Moreover, the NBO study was performed with the help of NBO3.1 package [33] at ωB97XD/6-311+G(d,p) level [34] as non-covalent interaction in a crystal can magnificently be analyzed at this level [35].The results were interpreted by utilizing GaussView 5.0 [36], GaussSum [37], Avogadro [38] and ChemCraft [39] software.

Molecular geometric parameters

Systematic computational optimization of **MBMHP, MABP, MBHP** and **MBCP** is done to measure structural parameters. The results of DFT and SC-XRD are found to be in a good agreement (Tables S1–S4), except some variations which might be due to the DFT computations being performed in gaseous phase and XRD done in solid phase. Overall, the variation in bond lengths are found within the range of 0.029 ± 0.008, 0.013 ± 0.007, 0.026 ± 0.002, and 0.013 ± 0.009 Å while in bond angles are in 1.4 ° ± 1.2°, 1.2 ° ± 0.9°, 1.4 ° ± 1.8° and 1.2 ° ± 1.2° in **MBMHP, MABP, MBHP** and **MBCP** respectively.

In **MBMHP** and **MABP** bond lengths for C-C in benzene rings are obtained within the range of 1.381-1.46 Å, 1.379-1.413 Å (XRD), while simulated values are examined to be 1.389-1.45 Å, 1.379-1.408 Å respectively. Similarly, the C-C bond lengths in benzene rings for **MBHP** and **MBCP** are obtained as 1.377-1.404 Å, 1.387-1.411 Å through XRD and 1.379-1.403 Å, 1.39-1.411 Å through DFT, respectively as shown in Tables S1–S4. In **MBMHP** bond lengths for O1-C7, O2-C8, O3-C16 and O4-C19 are obtained as 1.38, 1.364, 1.224 and 1.427 Å (XRD), while simulated values are explored to be 1.359, 1.353, 1.217 and 1.407 Å, respectively. (Table S1). For **MABP,** bond lengths for O1-C3, N2-C12, N2-C15 and N2-C16 are detected to be 1.223, 1.367, 1.448 and 1.447 Å (SC-XRD), whereas the calculated values of aforesaid bond lengths are measured as 1.21, 1.374, 1.444 and 1.443 Å, respectively as shown in Table S2. Furthermore, for **MBMHP** the bond lengths in C14-C15, C15-C19, C16-C17 and C17-C18 are seen as 1.342, 1.5, 1.495 and 1.503 Å (XRD), whereas the DFT investigated data of aforementioned bond lengths are observed as 1.342, 1.5, 1.491, and 1.502 Å, respectively as shown in Table S1. Similarly, for **MABP** the bond lengths in C3-C7, C5-C6, C7-C8, and C8-C9 are seen as 1.481, 1.544, 1.348, and 1.456 Å (XRD). On the other hand, the computationally explored data of aforesaid bond lengths are determined as 1.482, 1.537, 1.345 and 1.445 Å, respectively as shown in Table S2.

In **MBHP,** bond lengths O1-C6, O2-C7, O3-C15 and O4-C18 have been observed as 1.379, 1.367, 1.425 and 1.216 Å (SC-XRD), whereas the simulated values of aforementioned bond lengths are calculated as 1.359, 1.352, 1.406 and 1.211 Å, respectively (Table S3). Similarly, the bond length in **MBCP** is 1.218 Å for O1-C2 as noted by XRD, while the explored values of aforesaid bond length is obtained as 1.207Å, as shown in Table S4. Moreover, for **MBHP** the bond lengths in C13-C14, C14-C15, C14-C18, and C16-C17 are observed as 1.34, 1.514, 1.498 and 1.515 Å, whereas simulated bond lengths yielded 1.344, 1.507, 1.493 and 1.515 Å, respectively. Furthermore, for **MBCP** the bond lengths in C2-C3, C3-C4 and C7-C8 are seen as 1.506, 1.532 and 1.469 Å (XRD), whereas the DFT examined data of aforesaid bond lengths are found as 1.515, 1.524 and 1.456 Å, respectively. From above discussion it may be concluded that simulated and experimental bond lengths are found in well correlation.

In **MBMHP**, the bond angles such as C7-C6-C11=118.4°, C6-C7-C8=121°, C6-C11-C10=120.3° and C9-C10-C11= 121° are explored by XRD, whereas the simulated explored values of aforesaid bond angles are found as 118.7, 120.5, 120.5 and 120.7° respectively. Similarly, the bond angles: C7-O1-C12= 114.5°, O1-C7-C8= 119.7°, O2-C8-C7= 115.8° and O3-C16-C17= 121.4° are observed by SC-XRD, whereas the investigated values of aforesaid bond angles are seen as 115.2, 120.2, 116 and 121.8°, respectively. Furthermore, for **MABP** the bond angles like C4-C3-C7= 108.6°, C3-C7-C8= 120.2°, C6-C7-C8=131.1°, C8-C9-C14= 124.2°and C11-C12-C13= 117.1° are found by XRD, nevertheless the theoretical values of bond angles are determined as 107.4, 119.7, 131.5, 124.6 and 117.2°, respectively. The bond angles: O1-C3-C4= 125°, O1-C3-C7= 126.3°, C12-N2-C15= 120.9°, N2-C12-C11= 121.6° and C15-N2-C16= 118.4° are found (XRD) whereas the computed values of aforesaid bond angles are found as 125.7, 126.9, 119.9, 121.4 and 119.3°, respectively. (Tables S1–S2)

In **MBHP**, the bond angle values in C6-C5-C10=118.5°, C5-C6-C7=120.8°, C5-C10-C9=120.6°, C7-C8-C9=119.9° and C15-C14-C18=117.8° are found by (XRD), whereas the aforementioned bond angles are observed as 118.7, 120.6, 120.5, 119.9 and 118.1° (DFT) respectively. Similarly, the values of bond angles in C6-O1-C11=113.3°, O1-C6-C5=118.5°, C7-O2-C12=117.5°, O2-C7-C8=124.6° and C15-O3-C16=109.9° were observed by SC-XRD, while the computed values are determined as 115.1, 119.2, 118.2, 124.6 and 111.3°, respectively. Similarly, for **MBCP** values of bond angles in C2-C6-C7=120.3°, C4-C5-C6=104°, C9-C8-C13=118.9°and C10-C11-C12=119.3° are observed by (XRD), whereas theoretical values of bond angles are found to be 119.9, 103.8, 119 and 119.7°, respectively. Furthermore, the bond angles in O1-C2-C3=126.2° and O1-C2-C6=125.3° as observed by (XRD). On the other hand the calculated values of aforesaid bond angles are found as 126.2 and 126.5°, respectively. (Tables S3– S4) The above discussion describes that a tremendous understanding is found in experimental and DFT findings.

Natural bond orbital (NBO) analysis

NBO exploration has been viewed as one of the most relevant method that plays a crucial role in the study of intra and intermolecular H-bonding [40,41]. Besides, it exhibited an impressive understanding of the interaction and charge transfer processes of molecules. The second order stabilization energy ($E^{(2)}$) determin-

ing the strength of interaction within donor and acceptor, filled orbitals and the empty orbitals can be clarified by the NBO investigations [42,43]. $E^{(2)}$ can be described by the Eq. (1),

$$E^{(2)} = q_i \frac{(F_{ij})^2}{\varepsilon_j - \varepsilon_i} \quad (1)$$

Where q_i is donor orbital occupancy, ε_j and ε_i are diagonal elements and $F_{(i,j)}$ is off-diagonal NBO fock matrix element [44].

Some prominent $\pi \rightarrow \pi^*$ transitions are seen like: π(C39-C41)$\rightarrow\pi^*$(C36-C37), π(C19-C21)$\rightarrow\pi^*$(C16-C17), π(C7-C8)$\rightarrow\pi^*$(C10-C12), π(C22-C24)$\rightarrow\pi^*$(C18-C20) having higher stabilization energies as 40.90, 47.13, 34.91 and 37.82 *kcal/mol* in **MBMHP, MABP, MBHP** and **MBCP** respectively. Furthermore, $\sigma \rightarrow \sigma^*$ transitions are found as σ(C9-H10)$\rightarrow\sigma^*$(O2-C19), σ(C19-H20) $\rightarrow\sigma^*$(N2-C26), σ(C28-H29)$\rightarrow\sigma^*$(C25-H26), and σ(C12-C13)$\rightarrow\sigma^*$(C6-C9), showing lower stabilization energies: 0.5, 0.5, 0.51, 0.5 *kcal/mol*, respectively, for MBMHP, MABP, MBHP and MBCP as shown in Tables S5–S8.

Furthermore, for **MBMHP,** the $\pi \rightarrow \pi^*$ hyper-conjugative interactions are found like π(C42-C44)$\rightarrow\pi^*$(C39-C41), π(C8-C9)$\rightarrow\pi^*$(C6-C7) and π(C42-C44)$\rightarrow\pi^*$(C36-C37) with stabilization energies: 36.95, 29.86 and 26.83 *kcal/mol*, respectively. The conjugative interactions ($\sigma \rightarrow \sigma^*$) are determined as σ(C46-H49)$\rightarrow\sigma^*$(O2-C19), σ(O5-C41)$\rightarrow\sigma^*$(C15-H16), and σ(C46-H49)$\rightarrow\sigma^*$(C25-C26), with stabilization energies as 147.14, 103.38, and 77.72, *kcal/mol*, respectively. Similarly, for **MABP,** the $\pi \rightarrow \pi^*$ hyper-conjugative interactions are found like π(C16-C17)$\rightarrow\pi^*$(C22-C24), π(C22-C24)$\rightarrow\pi^*$(C19-C21) and π(C13-C14)$\rightarrow\pi^*$(O1-C3) with stabilization energies: 38.44, 33.68 and 30.76 *kcal/mol*, respectively. The conjugative interactions ($\sigma \rightarrow \sigma^*$) are noticed as σ(C30-H31)$\rightarrow\sigma^*$(C30-H33), σ(N2-C30)$\rightarrow\sigma^*$(C30-H33) and σ(C14-H15)$\rightarrow\sigma^*$(C10-C13), with stabilization energies as 33.86, 19.79, and 8.69, *kcal/mol*, respectively. For **MBMHP,** the LP$\rightarrow\sigma^*$ interactions are recognized as LP(1)-O3$\rightarrow\sigma^*$(C15-H16), LP(1)-O3$\rightarrow\sigma^*$(C46-H47) and LP(1)-O2 $\rightarrow\sigma^*$(C25-C26) with stabilization energies: 1214.38, 146.7 and 28.04 *kcal/mol*, respectively as shown in Tables S5-S8. Similarly, the LP$\rightarrow\pi^*$ transitions have been seen as LP(1)-O3$\rightarrow\pi^*$(C23-C25), LP(2)-O5$\rightarrow\pi^*$(C39-C41) with stabilization energies: 330.33 and 42.04 *kcal/mol*, respectively. Similarly, for **MABP,** the LP$\rightarrow\sigma^*$ interactions are recognized as LP(2)-O1$\rightarrow\sigma^*$(C3-C4), LP(2)-O1$\rightarrow\sigma^*$(C3-C13) and LP(1)(N2)$\rightarrow\sigma^*$(C26-H28), with stabilization energies: 27.21, 24.49 and 7.88 *kcal/mol*, respectively as shown in Tables S5–S8. Moreover, the LP$\rightarrow\pi^*$ transitions are seen as LP(1)(N2)$\rightarrow\pi^*$(C19-C21) with stabilization energy; 60.6 *kcal/mol.*

In **MBHP** the $\pi \rightarrow \pi^*$ transitions are observed as π(C5-C6)$\rightarrow\pi^*$(C10-C12), π(C10-C12)$\rightarrow\pi^*$(C7-C8) and π(C22-C24)$\rightarrow\pi^*$(O4-C34) with stabilization energies: 30.56, 29.83 and 28.12 *kcal/mol*, respectively as shown in Tables S5–S8. Similarly, for **MBCP,** the $\pi \rightarrow \pi^*$ hyper-conjugative interactions are found like π(C18-C20)$\rightarrow\pi^*$(C15-C16), π(C15-C16)$\rightarrow\pi^*$(C18-C20) and π(C15-C16)$\rightarrow\pi^*$(C22-C24) with stabilization energies: 37.45, 33.62 and 33.36 *kcal/mol*, respectively. The $\sigma \rightarrow \sigma^*$ transitions for **MBHP** are determined as σ(O4-C34)$\rightarrow\sigma^*$(C31-H33), σ(C24-C34)$\rightarrow\sigma^*$(C28-H30) and σ(C31-H32)$\rightarrow\sigma^*$(O4-C34) with stabilization energies as 127.59, 18.48 and 10.41 *kcal/mol*, respectively. Furthermore for **MBCP** some important $\sigma \rightarrow \sigma^*$ transitions like σ(C13-H14)$\rightarrow\sigma^*$(C9-C12), σ(C25-H26)$\rightarrow\sigma^*$(C15-C24) and σ(C13-C15)$\rightarrow\sigma^*$(C12-C13) are seen with stabilization energies as 9.86, 5.33 and 4.97*kcal/mol* respectively as shown in Tables S5–S8. For **MBHP**, the LP$\rightarrow\sigma^*$ hyper-conjugative interactions like LP(1)-O4$\rightarrow\sigma^*$(C31-H33), LP(2)-O4$\rightarrow\sigma^*$(C28-H30) and LP(2)-O4$\rightarrow\sigma^*$(C31-C34) with stabilization energies: 44.52, 30.69 and 19.21 *kcal/mol.* While the LP$\rightarrow\pi^*$ transitions has been seen as LP(1)-O1$\rightarrow\pi^*$(C5-C6) with stabilization energy 9.16 *kcal/mol* as shown in Tables S5–S8. For **MBCP** some significant LP-σ^* conjugative interactions are also observed as LP(2)-O1$\rightarrow\sigma^*$(C2-C3), LP(2)-O1$\rightarrow\sigma^*$(C2-C12), LP(1)-O1$\rightarrow\sigma^*$(C2-C12) and LP(1)-O1$\rightarrow\sigma^*$(C2-C3) yielding stabilization energies as 27.07, 25.13, 2.55 and 1.88 *kcal/mol,* respectively. The transition from $\sigma \rightarrow \pi^*$ is observed as σ(C46-H49)$\rightarrow\pi^*$(C23-C25), σ(C4-H5)$\rightarrow\pi^*$(O1-C3), σ(C31-H33)$\rightarrow\pi^*$(O4-C34) and σ(C9-H10)$\rightarrow\pi^*$(C12-C13) with stabilization energies; 5822.67, 9.36, 2.35 and 6.58 *kcal/mol* for **MBMHP, MABP, MBHP** and **MBCP**, respectively, as shown in Tables S5–S8. From above analysis it could be concluded that the stronger intra-molecular hyper-conjugation are responsible for the stability of the title compounds.

Natural population analysis (NPA)

Electrical potentials, NMR chemical shifts, dipole moments and electromagnetic spectra were favorable parameters to reveal molecular properties which correlate reasonably to atomic charges in the organic compounds [45]. The scientific reports related to structural characteristics of chemical compounds abundantly rely on atomic charges concept [46]. The characterization of atomic charges could be helpful to understand the non-covalent interaction pattern in any chemical structure [47].

Frontier molecular orbital analysis

Frontier molecular orbital energies and their band gaps are contemplated as very viable parameters in quantum chemistry [48,49].HOMO and LUMO energies specify nucleophilic and electrophilic characters, respectively [50].Moreover, FMOs play a vital role in discovering optical and electrical properties, chemical reactivity, and intermolecular interactions for various compounds. Literature shows that a greater HOMO-LUMO gap is associated with higher stability and lower reactivity of compounds [51].HOMO-LUMO low energy gap accounts for a lower stability and higher reactivity of compounds with remarkable NLO properties. The study of FMOs was carried out and results are shown in Table S9.

The energy gap for the title molecules namely **MBMHP, MABP, MBHP** and **MBCP** are 4.144, 4.127, 4.768, and 4.762 *eV,* respectively. The overall diminishing order of the band gap is obtained to be **MBHP**>**MBCP**>**MBMHP**>**MABP**, showing that the energy gap of the **MABP** is less than all the other crystals showing greater reactivity and more efficient intra-molecular charge transfer (ICT), whereas the **MBHP** shows less reactivity and hence is more stable. The FMO contour surfaces are showing the pattern of the density circulation of electrons and the transmission of charge in HOMO and LUMO. For **MBMHP**, the HOMO is populated on the (*E*)-3-(4-methoxybenzylidene) tetrahydro-4H-pyran-4-one moiety and small effect exist on some other carbon atoms while, the LUMO is occupied on the ((*E*)-2-benzylidene)-5-((*E*)-4-hydroxybenzylidene)tetrahydro-4*H*-pyran-4-one moiety but small effect on both benzene carbon atoms (Fig. 4). While for **MABP**, the HOMO has been populated on the entire molecule except some carbon atoms of cyclopentane group whereas; the LUMO is also populated on the entire molecule except both methyl groups and some carbon atoms of benzene ring (Fig. 4). Nevertheless, for **MBHP** the HOMO is populated on the (Z)-3-(2,3-methoxybenzylidene) moiety and small effect exist on some carbons and oxygen atom of tetrahydro-4H-pyran-4-one moiety whereas, the LUMO is located on the (Z)-3-benzylidenetetrahydro-4*H*-pyran-4one moiety except on some carbons and oxygen atom of tetrahydro-4H-pyran-4-one moiety (Fig. 4).

For **MBCP**, the HOMO is located on the (E)-2-(2-methylbenzylidene)cyclopentan-1-one except some carbon atoms of cyclopentane ring and small contribution is made by the methyl group whereas the LUMO is also located on the entire molecule except some carbon atoms of cyclopentane ring and methyl group (Fig. 4).

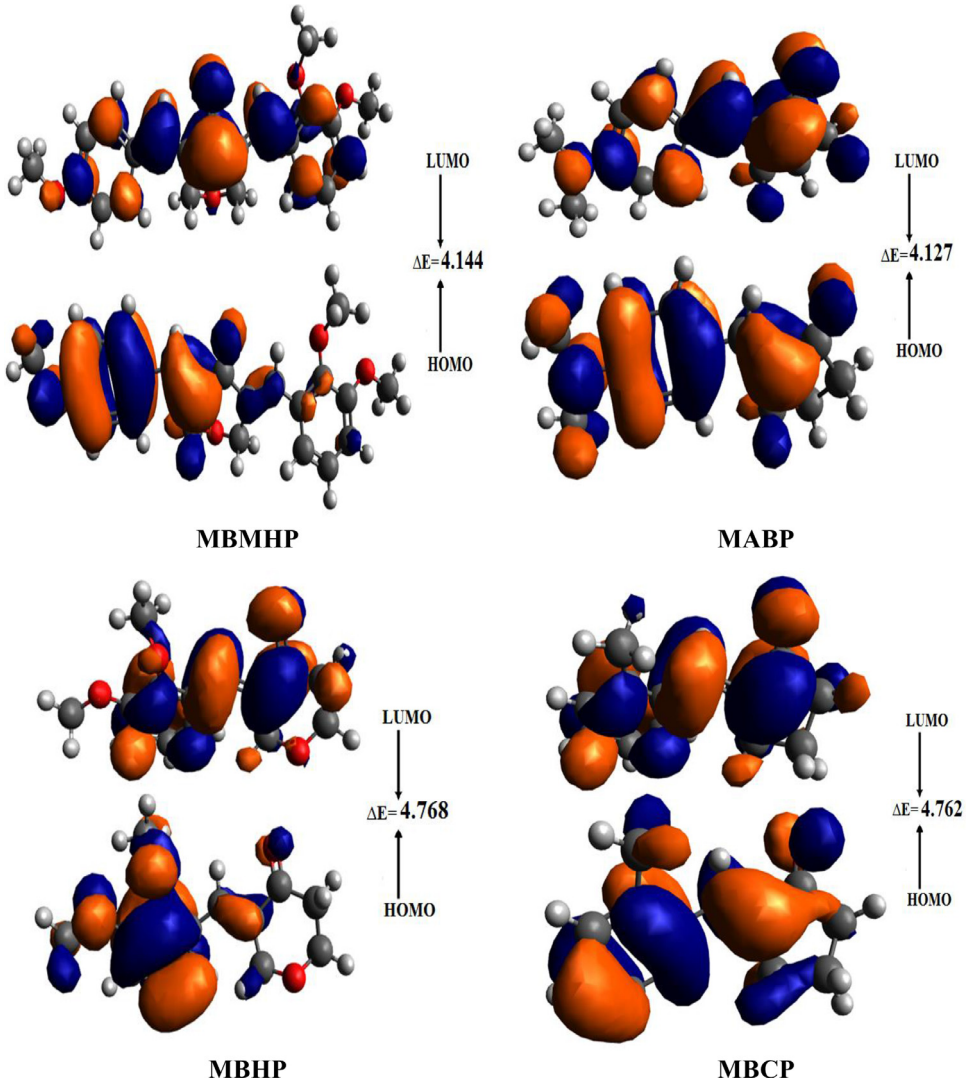

Fig. 4. Frontier molecular orbitals of title compounds.

The energy gaps between HOMO and LUMO help to derive parameters used to describe stability and reactivity by evaluating global reactivity parameters [52]. The values of these parameters, including Ionization potential (*IP*) [53], electron affinity (*EA*), global electrophilicity (ω) [54, 55] global hardness (η)[56,57], electronegativity (X)[58],chemical potential (μ)[59], and global softness [60] (σ) are determined by the EqS. (2)–(3), and their results are evaluated in Table S10.

$$IP = -E_{HOMO} \tag{2}$$

$$EA = -E_{LUMO} \tag{3}$$

Where IP = ionization potential (eV), EA = electron affinity (eV).

Koopmans's theorem [61] has been used to calculated the the electronegativity (X), the chemical potential (μ) and the chemical hardness by using Eqs. (4)–(7).

$$X = \frac{[IP + EA]}{2} = -\frac{[E_{LUMO} + E_{HOMO}]}{2} \tag{4}$$

$$\eta = \frac{[IP - EA]}{2} = -\frac{[E_{LUMO} - E_{HOMO}]}{2} \tag{5}$$

$$\mu = \frac{E_{HOMO} + E_{LUMO}}{2} \tag{6}$$

For global softness (σ) following equation was used.

$$\sigma = \frac{1}{2\eta} \tag{7}$$

By Parr et al. the calculation of electrophilicity index (ω) is performed using Eq. (8) [62].

$$\omega = \frac{\mu^2}{2\eta} \tag{8}$$

The ability to lose or gain electrons of the title compounds is categorized by their ionization potential and the electron affinity values, respectively. The compound **MBCP** has the maximum *IP* value of 6.742 *eV*, while **MABP** has the minimum value of 5.746 *eV* (Table S10) The **MBMHP** crystal possessed highest *EA* value; 2.181 *eV* while **MABP** contained least *EA* value; 1.619 *eV*. Moreover, the *IP* values of all the four compounds are analyzed lower in extent than *EA* values which showed that the studied molecules contained excellent electron-donating ability. In addition, chemical potential values (μ) have been taken into account for the understanding of the stability and reactivity of any molecule, which indicates that compound with lesser chemical potential is favored as less steady and reactive compound or vice versa. In investigated compounds, the chemical potential values decreasing order given as, -4.361 > -4.336 > -4.253 > -3.6825 which indicates that **MBCP** is highly reactive compound (Table S10)

Table 3
Computated polarizabilities and hyperpolarizability of title compounds.

Compounds	$<\alpha>$	$<\gamma>$
MBMHP	379.41	8.96×105
MABP	281.60	5.70×105
MBHP	216.36	1.06×104
MBCP	218.37	1.64×105

Nonlinear optical (NLO) properties

The investigation of compounds with extraordinary NLO properties is a vast area of exploration because of their flexible use in optoelectronics and telecommunications [63,64]. The concepts of polarizability $<\alpha>$ and second hyper polarizability $<\gamma>$ in NLO studies are used to clarify the structure-property relationships with the assistance of quantum chemical calculations. Herein, the $<\alpha>$ and $<\gamma>$ of MBMHP, MABP, MBHP and MBCP are calculated at M06 level and results are tabulated in Tables S11,S12 while some important results are shown in Table 3.

Table 3 illustrated that the least value for linear polarizability $<\alpha>$ and second order hyperpolarizability$<\gamma>$ is analyzed in **MBHP** to be 216.36 and 1.06×10^4 *a.u* respectively, among all the investigated molecules. This might be due that the methoxy group that along with the positive resonate effect (+*R*) also have negative inductive (-*I*) effect as by σ-bonds, it can withdraw the electron and lower the charge transfer, moreover the presence of tetrahydro-2H-pyran ring which is not planar ring also decreased the conjugation hence, a powerful push pull architecture does created so exhibit lower NLO responses. These values increase to 218.37 and 1.64×10^5 *a.u*, in **MBCP** than enlarge to 281.60 and 5.70×10^5 *a.u* in **MABP** for $<\alpha>$ and $<\gamma>$ respectively, as the conjugation extended. However, the highest value of linear polarizability and second order hyperpolarizability is examined in **MBMHP** which is 379.41 and 8.960×10^5 *a.u* respectively, among all entitled compounds. This might be due to that in **MBMHP** the no of atom increased as the polarizability naturally grows with the number of atoms in the molecules. Additionally, the extended conjugation and D-π-A-π-D type structure created a strong push pull mechanism in this molecule, hence shows excellent NLO results. The overall decreasing order of $<\alpha>$ and $<\gamma>$ is: **MBMHP > MABP > MBCP > MBHP.** This urea comparative study suggested that all molecules under investigation are suitable NLO candidates.

Conclusions

The crystalline monoarylidene and unsymmetrical diarylidene alkanones are prepared using the Aldol condensation reaction. The title compounds are characterized by the nuclear magnetic spectroscopic techniques and single crystal analysis. According to SC-XRD investigation all the compounds, **MBMHP, MABP** and **MBHP** exhibit $P2_1/c$ space group with monoclinic crystal system except **MBCP** that has orthorhombic, crystal system and *Aba*2 space group. To stabilize the structure of crystals in solid state, the role of different non-covalent interactions is also discussed. Moreover, the NBO investigations revealed that the intra molecular and hyper conjugation charge transfer also plays a significant role to stabilize the molecule. Furthermore, the NPA study also proposed the non-covalent interactions in the entitled compounds that endorsed the determination of SC-XRD investigations. With the help of FMOs the charge transfer and chemical reactivity of molecules under analysis is discussed. Besides these GRP have also been determined from the energies of HOMO/LUMO. Among all crystals **MBHP** has higher value of hardness (η = 2.384 *eV*) while **MABP** showed higher global softness (σ=0.242307 *eV*). So, from GRP it is revealed that all the studied crystals are less reactive and more stable as suggested by NBO and SC-XRD investigations. NLO study described that the crystal **MBMHP** have the higher value of linear polarizability $<\alpha>$ and third order polarizability$<\gamma>$ 216.36 and 1.06×10^4 *a.u* respectively, among all the synthesized crystals. The simulated structural parameters of aforesaid crystals and experimental X-ray crystallographic determinations are established in a close harmony. All the four compounds disclosed remarkable NLO responses which can be notable for their utilization in advanced applications.

Declaration of Competing Interest

The authors declare that they have no known competing financial interests or personal relationships that could have appeared to influence the work reported in this paper.

Acknowledgment

M. Imran express appreciation to the Deanship of Scientific Research at King Khalid University Saudi Arabia for funding through research groups program under grant number R.G.P. 2/28/42.

Supplementary materials

Supplementary material associated with this article can be found, in the online version, at doi:10.1016/j.molstruc.2021.130685.

References

[1] Z.U. Din, T.P Fill, F.F. Assis, D. L-Bidóia, V. Kaplum, F.P. Garcia, C.V. Nakamurab, K.T. Oliveira, E. R-Filho, Unsymmetrical 1,5-diaryl-3-oxo-1,4-pentadienyls and their evaluation as antiparasitic agents, Bioorg. Med. Chem. 22 (2014) 1121–1127.
[2] H. Patel, B. Mothia, J. Patel, O. Fasanya, K. Sooda, F. Javid, P.B. Wyatt, Cytotoxicity of some synthetic bis(arylidene) derivatives of cyclicketones towards cisplatin-resistant human ovarian carcinoma cells, Med. Chem. Res. 29 (2020) 935–941.
[3] (a) Y. Zhang, Z. Liu, J. Wu, B. Bai, H. Chen, Z. Xiao, L. Chen, Y. Zhao, H. Lum, Y. Wang, H. Zhang, G. Liang, New MD2 inhibitors derived from curcumin with improved anti-inflammatory activity, Eur. J. Med. Chem. 148 (2018) 291–305; (b) A. Araico, M.C. Terencio, M.J. Alcaraz, J.N. Domínguez, C. León, M.L. Ferrándiz, Evaluation of the anti-inflammatory and analgesic activity of Me-UCH9, a dual cyclooxygenase-2 /5-lipoxygenase inhibitor, Life Sci. 80 (2007) 2108–2117.
[4] D. Batovska, S. Parushev, B. Stamboliyska, I. Tsvetkova, Examination of growth inhibitory properties of synthetic chalcones for which antibacterial activity was predicted, Eur. J. Med. Chem. 44 (2009) 2211–2218.
[5] a) R. De, P. Kundu, S. Swarnakar, T. Ramamurthy, A. Chowdhury, G.B. Nair, A.K. Mukhopadhyay, Antimicrobial activity of curcumin against Helicobacter pylori isolates from India and during infections in mice, Antimicrob. Agents Chemother. 53 (2009) 1592–1597; b) Z.U. Din, N.F.G. Serrano, K. Ademi, C.P. Sousa, V.M. Deflon, P. ld. S. Maia, E. R-Fillho, Crystal structures, in-silico study and anti-microbial potential of synthetic monocarbonyl curcuminoids, J. Mol. Struct. 1144 (2017) 529–534.
[6] a) A. Mascarello, L.D. Chiaradia, J. Vernal, A. Villarino, R.V.C. Guido, P. Perizzolo, V. Poirier, D. Wong, P.G.A. Martins, R.J. Nunes, R.A. Yunes, Y.Av-G A.D.Andricopulo, H. Terenzi, Inhibition of Mycobacterium tubercusis tyrosine phosphatase PtpA by synthetic chalcones: kinetics, molecular modeling, toxicity and effect on growth, Bioorg. Med. Chem. 18 (2010) 3783–3789; b) R.B. Aher, G. Wanare, N. Kawathekar, R.R. Kumar, N.K. Kaushik, D. Sahal, V.S. Chauhan, Dibenzylideneacetone analogues as novel Plasmodium falciparum inhibitors, Bioorg. Med. Chem. 21 (2011) 3034–3036.
[7] L.L. Franco, M.V. de Almeida, L.F.R.E Silva, P.P.R. Vieira, A.M. Pohlit, M.S. Valle, Synthesis and antimalarial activity of dihydroperoxides and tetraoxanes conjugated with bis(benzyl)acetone derivatives, Chem. Biol. Drug Des. 79 (2012) 790–797.
[8] K.L. Lahtchev, D.I. Batovska, S.P. Parushev, V.M. Ubiyvovk, A.A. Sibirny, Antifungal activity of chalcones: a mechanistic study using various yeast strains, Eur. J. Med. Chem. 43 (2008) 2220–2228.
[9] R. Gacche, M. Khsirsagar, S. Kamble, B. Bandgar, N. Dhole, K. Shisode, A. Chaudhari, Antioxidant and anti-inflammatory related activities of selected synthetic chalcones: structure – activity relationship studies using computational tools, Chem. Pharm. Bull. 56 (2008) 897–901.
[10] Y. Lv, A. LAN, C. LI, N. LEI, C. WU, L. LIU, Activity of curcumin against human cytomegalovirus in vitro, Afr. J. Pharm. Pharmacol. 6 (2012) 30–35.
[11] S. Ducki, R. Forrest, J.A. Hadfield, A. Kendall, N.J. Lawrence, A.T. McGown, D. Rennison, Potent antimitotic and cell growth inhibitory properties of substituted chalcones, Bioorg. Med. Chem. Lett. 8 (1998) 1051–1056.

[12] H. Zhang, J-J. Liu, J. Sun, X-H. Yang, T-T. Zhao, X. Lu, H-B. Gong, H-L. Zhu, Design, synthesis and biological evaluation of novel chalcone derivatives as antitubulin agents, Bioorg. Med. Chem. 20 (2012) 3212–3218.

[13] M. Cabrera, M. Simoens, G. Falchi, M.L. Lavaggi, O.E. Piro, E.E. Castellano, A. Vidal, A. Azqueta, A. Monge, A.L. Ceráin, G. Sagrere, G. Seoane, H. Cerecetto, M. González, Synthetic chalcones, flavanones, and flavones as antitumoral agents: biological evaluation and structure-activity relationships, Bioorg. Med. Chem. 15 (2007) 3356–3367.

[14] I.H. Hall, G.L. Carlson, G.S. Abernethy, C. Piantadosi, Cycloalkanones. Antifertility activity, J. Med. Chem. 17 (1974) 1253–1257.

[15] a) S.F.P. Braga, É.V.P. Alves, R.S. Ferreira, J.R.B. Fradico, P.S. Lage, M.C. Duarte, T.G. Ribeiro, P.A.S. Júnior, A.J. Romanha, M.L. Tonini, M. Steindel, E.F. Coelho, R.B. Oliveira, Synthesis and evaluation of the antiparasitic activity of bis-(arylmethylidene) cycloalkanones, Eur. J. Med. Chem. 71 (2014) 282–289; b) D.L. Bidóia, V.C. Desoti, S.C. Martins, F.M. Ribeiro, Z.U. Din, E. R.-Filho, T. U–Nakamura, C.V. Nakamura, S.O. Silva, Dibenzylideneacetones are potent trypanocidal compounds that affect the Trypanosoma cruzi redox system, Antimicrob. Agents Chemo. 60 (2016) 890–903; c) S. Attar, Z. O'Brien, H. Alhaddad, M.L. Golden, A. Calderón-Urrea, Ferrocenyl chalcones versus organic chalcones: a comparative study of their nematocidal activity, Bioorg. Med. Chem. 19 (2011) 2055–2073.

[16] a) R.J. Anto, K. Sukumaran, G. Kuttan, M.N.A. Rao, V. Subbaraju, R. Kuttan, Anticancer and antioxidant activity of synthetic chalcones and related compounds, Cancer Lett. 97 (1995) 33–37; b) M.L. Go, X. Wu, X.L. Liu, Chalcones: an update on cytotoxic and chemoprotective properties, Curr. Med. Chem. 12 (2005) 483–499; c) S. Prasad, V.R. Yadav, J. Ravindran, B.B. Aggarwal, ROS and CHOP are critical for dibenzylideneacetone to sensitize tumor cells to TRAIL through induction of death receptors and downregulation of cell survival proteins, Cancer Res. 71 (2011) 538–549.

[17] S.W. Leong, S.M.M. Faudzi, F. Abas, M.F.F.M. Aluwi, K. Rullah, L.K. Wai, M.N.A. Bahari, S. Ahmad, C.L. Tham, K. Shaari, N.H. Lajis, Synthesis and SAR study of diarylpentanoid analogues as new anti-inflammatory agents, Molecules 19 (2014) 16058–16081.

[18] S.F.P. Braga, É.V.P. Alves, R.S. Ferreira, J.R.B. Fradico, P.S. Lage, M.C. Duart, T.G. Ribeiro, P.S. Júnior, A.J. Romanha, M.L. Tonini, M. Steindel, E.F. Coelho, R.B. Oliveira, Synthesis and evaluation of the antiparasitic activity of bis-(arylmethylidene) cycloalkanones, Eur. J. Med. Chem. 71 (2014) 282–289.

[19] C.A. Zoto, RE. Connors, Photophysical properties of an asymmetrical 2,5-diarylidene-cyclopentanonedye possessing electron donor and acceptor substituents, J. Mol. Struct. 982 (2010) 121–126.

[20] (a) M. Khalid, A. Ali, R. Jawaria, M.A. Asghar, S. Asim, M.U. Khan, R. Hussain, M.F. Rehman, C.J. Ennis, M.S. Akram, First principles study of electronic and nonlinear optical properties of A-D–π–A and D-A-D–π–A configured compounds containing novel quinoline-carbazole derivatives, RSC Adv. 10 (2020) 22273–22283; (b) S. Tariq, A.R. Raza, M. Khalid, S.L. Rubab, M.U. Khan, A. Ali, M.N. Tahir, A.A.C. Braga, Synthesis and structural analysis of novel indole derivatives by XRD, spectroscopic and DFT studies, J. Mol. Struct. 1203 (2020) 127438; (c) A. Ali, M. Khalid, K.P. Marrugo, G.M. Kamal, M. Saleem, M.U. Khan, O. Concepción, A.F. delaTorre, Spectroscopic and DFT/TDDFT insights of the novel phosphonate imine compounds, J. Mol. Struct. 1207 (2020) 127838.

[21] (a) M.G. Papadopoulos, A.J. Sadlej, J. Leszczynski, NONLINEAROPTICAL PROPERTIES OF MATTER, Springer, Dordrecht, 2006; (b) D.F. Eaton, NONLINEAR OPTICAL MATERIALS: THE GREAT AND NEAR GREAT, ACS Publications, 1991.

[22] S. Mukherjee, P. Thilagar, Organicwhite-light emitting materials, Dyes. Pigm. 110 (2014) 2–27.

[23] (a) S.V. Likhomanova, N.V. Kamanina, COANP-fullerenes system for opticalmodulation, J. Phys. Conf. Ser. 741 (2016) 012146; (b) M. Khalid, A. Ali, A.F. De la Torre, K.P. Marrugo, O. Concepcion, G.M. Kamal, S. Muhammad, A.G. Al-Sehemi, Facile synthesis, spectral (IR, Mass, UV-Vis, NMR), LINEAR AND NONLINEAR INVESTIGATION OF THE NOVEL PHOSPHONATE COMPOUNDS: A COMBINED EXPERIMENTAL AND SIMULATION STUDY, ChemistrySelect 5 (2020) 2994–3006.

[24] (a) M. Khalid, A. Ali, M. Adeel, Z.U. Din, M.N. Tahir, E.R. Filho, J. Iqbal, M.U. Khan, Facile preparation, characterization, SC-XRD and DFT/DTDFT study of diversely functionalized unsymmetrical bis-aryl-α,β-unsaturated ketone, J. Mol. Struct. 1206 (2020) 127755.

[25] Z.U. Din, E.R. Filho, Optimized one-pot synthesis of monoarylidene and unsymmetrical diarylidene cycloalkanones, Arab. J. Chem. 12 (2019) 4756–4763.

[26] M. J. Frisch, G. W. Trucks, H. B. Schlegel, G. Scuseria, M.A.Robb, J. R. Cheeseman, G. Scalmani, V. Barone, B. Mennucci, G. Petersson, H. Nakatsuji, M. Caricato, X. Li, H. P. Hratchian,A. F. Izmaylov, J. Bloino, G. Zheng, J. L. Sonnenberg, M. Hada, M. Ehara, K. Toyota, R. Fukuda, J. Hasegawa, M. Ishida, T. Nakajima, Y. Honda, O. Kitao, H. Nakai, T. Vreven, J. A. Montgomery, J. E. Peralta, F. Ogliaro, M. Bearpark, J. J. Heyd, B. E. K. N. Kudin, V. N. Staroverov, R. Kobayashi, J. Normand, K. Raghavachari, A. Rendell, J. C. Burant, S. S. Iyengar, J. Tomasi, M. Cossi, N. Rega, J. M. Millam, M. Klene, J. E. Knox, J. B. Cross, V. Bakken, C. Adamo, J. Jaramillo, R. Gomperts, R. E. Stratmann, O. Yazyev, A. J. Austin, R. Cammi, C. Pomelli, J. W. Ochterski, R. L. Martin, K. Morokuma, V. J. Zakrzewski, G. A. Voth, P. Salvador, J. J. Dannenberg, S. Dapprich, A. D. Daniels, O. Farkas, J. B. Foresman, J. V. Ortiz, J. Cioslowski, D. J. Fox, Gaussian 09, Revision B.01., Gaussian, Inc., Wallingford, (2009).

[27] A.A.C. Braga, G. Ujaque, F. Maseras, A DFT study of the full catalytic cycle of the Suzuki– Miyaura cross-coupling on a model system, Organometallics 25 (2006) 3647–3658.

[28] A.A.C. Braga, N.H. Morgon, G. Ujaque, F. Maseras, Computational characterization of the role of the base in the Suzuki– Miyaura cross-coupling reaction, J. Am. Chem. Soc. 127 (2005) 9298–9307.

[29] A.A.C. Braga, N.H. Morgon, G. Ujaque, A. Lledós, F. Maseras, Computational study of the transmetalation process in the Suzuki–Miyaura cross-coupling of aryls, J. Organomet. Chem. 691 (2006) 4459–4466.

[30] Frisch M., Trucks G., Schlegel H., Scuseria G., Robb M., Cheeseman J., Scalmani G., Barone V., Mennucci B. and Petersson G., in: Gaussian, Inc., Wallingford CT, 2009.

[31] Y. Zhao, D.G. Truhlar, Theor. The M06 suite of density functionals for main group thermochemistry, thermochemical kinetics, noncovalent interactions, excited states, and transition elements: two new functionals and systematic testing of four M06-class functional and 12 other functionals, Chem. Acc. 120 (2008) 215–241.

[32] A.A M.Khalid, M.F.U. Rehman, M. Mustaqeem, Exploration of noncovalent interactions, chemical reactivity, and nonlinear optical properties of piperidone derivatives: a concise theoretical approach, ACS Omega 5 (2020) 13236–13249.

[33]] F. Weinhold, E.D. Glendening, in: NBO 5.0 PROGRAM MANUAL: NATURAL BOND ORBITAL ANALYSIS PROGRAMS, THEORETICAL CHEMISTRY INSTITUTE AND DEPARTMENT OF CHEMISTRY, University of Wisconsin, Madison, WI, 2001, p. 53706.

[34] J.D. Chai, M. Head-Gordon, Long-range corrected hybrid density functionals with damped atom–atom dispersion corrections, Phys. Chem. Chem. Phys. 10 (2008) 6615–6620.

[35] A. Ali, M. Khalid, S. Abid, J. Iqbal, Facile synthesis, crystal growth, characterization and computational study of new pyridine-based halogenated hydrazones: Unveiling the stabilization behavior in terms of noncovalent interactions, Appl. Organomet. Chem. 34 (2019) 5399.

[36] R. Dennington, T. Keith, J. Millam, GaussView, version 5, Semichem Inc., Shawnee Mission, KS, 2009.

[37] http://gausssum.sourceforge.net/DocBook/pr02.html. [Accessed: 07-Apr-2019].

[38] http://avogadro.cc/wiki/Main_Page.

[39] A.E. Reed, F. Weinhold, R. Weiss, et al., Nature of the contact ion pair trichloromethyl-chloride (CCl^{3+} Cl^{-}). A theoretical study, J. Phys. Chem. 89 (1985) 2688–2694.

[40] A.E. Reed, F. Weinhold, R. Weiss, et al., Nature of the contact ion pair trichloromethyl-chloride (CCl^{3+} Cl^{-}). A theoretical study, J. Phys. Chem. 89 (1985) 2688–2694.

[41] M.N. Arshad, M.M Hussain, A.M Asiri, M. Khalid, A.A. Braga, A potent synthesis and supramolecular synthon hierarchy percipience of (E)-N′-(Napthalen-1-yl-methylene)-benzenesulfonohydrazide and 1-Napthaldehyde: A combined experimental and DFT studies, J. Mol. Struct. 1221 (2020) 128797.

[42] M. Szafran, A. Komasa, E.B. Adamska, Crystal and molecular structure of 4-carboxypiperidinium chloride (4-piperidinecarboxylic acid hydrochloride, J. Mol. Struct. 827 (2007) 101–107.

[43] C. James, A.A. Raj, R. Reghunathan, V.S. Jayakumar, I.H. Joe, Structural conformation and vibrational spectroscopic studies of 2, 6-bis (p-N, N-dimethyl benzylidene) cyclohexanone using density functional theory, J. Raman Spectrosc. 37 (2006) 1381–1392.

[44] J.N. Liu, Z.R. Chen, S.F. Yuan, Study on the prediction of visible absorption maxima of azobenzene compounds, J. Zhejiang Univ. Sci. B 6 (2005) 584.

[45] E. Khan, A. Khan, Z. Gul, F. Ullah, M.N. Tahir, M. Khalid, H.M. Asif, S. Asim, A.A.C. Braga, Molecular salts of terephthalic acids with 2-aminopyridine and 2-aminothiazole derivatives as potential antioxidant agents; Base-Acid-Base type architectures, J. Mol. Struct. 1200 (2020) 127126.

[46] M. Khalid, A. Ali, M. Adeel, Z.U. Din, M.N. Tahir, E.R. Filho, J. Iqbal, M.U. Khan, Facile preparation, characterization, SC-XRD and DFT/DTDFT study of diversely functionalized unsymmetrical bis-aryl-α, β-unsaturated ketone derivatives, J. Mol. Struct. 1206 (2020) 127755.

[47] E. Khan, M. Khalid, Z. Gul, A. Shahzad, M.N. Tahir, H.M. Asif, S. Asim, A.A.C. Braga, Molecular structure of 1, 4-bis (substituted-carbonyl) benzene: A combined experimental and theoretical approach, J. Mol. Struct. 1205 (2020) 127633.

[48] M.N. Arshad, A.A.M.A. Dies, A.M. Asiri, M. Khalid, A.S. Birinji, K.A.A. Amry, A.A.C. Braga, Synthesis, crystal structures, spectroscopic and nonlinear optical properties of chalcone derivatives: a combined experimental and theoretical study, J. Mol. Struct. 1141 (2017) 142–156.

[49] M.N. Tahir, M. Khalid, A. Islam, S.M.A. Mashhadi, A.A.C. Braga, Facile synthesis, single crystal analysis, and computational studies of sulfanilamide derivatives, J. Mol. Struct. 1127 (2017) 766–776.

[50] M. Khalid, M. Ali, M. Aslam, S.H. Sumrra, M.U. Khan, N. Raza, N. Kumar, M. Imran, Frontier molecular, natural bond orbital, UV–Vis spectral study, solvent influence on geometric parameters, vibrational frequencies and solvation energies of 8-hydroxyquinoline, Int. J. Pharm. Sci. Res. 8 (2017) 457.

[51] S. Tariq, M. Khalid, A.R. Raza, S.L. Rubab, S.F.A. Morais, M.U. Khan, M.N. Tahir, A.A.C. Braga, Experimental and computational investigations of new indole derivatives: a combined spectroscopic, SC-XRD, DFT/TD-DFT and QTAIM analysis, J. Mol. Struct. 1207 (2020) 127803.

[52] R.G. Parr, L.V. Szentpaly, S. Liu, Electrophilicity index, J. Am. Chem. Soc. 121 (1999) 1922–1924.

[53] C.G. Zhan, J.A. Nichols, D.A. Dixon, Ionization potential, electron affinity, electronegativity, hardness, and electron excitation energy: molecular properties from density functional theory orbital energies, J. Am. Chem. Soc. 107 (2003) 4184–4195.

[54] (a) R. Parthasarathi, V. Subramanian, D.R. Roy, P.K. Chattaraj, Electrophilicity index as a possible descriptor of biological activity, Bioorg. Med. Chem. 12 (2004) 5533–5543; (b)Chattaraj, P.K., <? ACS-CT-START-Insert?>Giri<? ACS-CT-END-Insert?>, A. C. S. I. S. A. C. E. I., &<? ACS-CT-START-Insert?>Duley<? ACS-CT-END-Insert?>, A. C. S. I. S. A. C. E. I. (2011). <? ACS-CT-START-Insert?>Update 2 of:<? ACS-CT-END-Insert?> Electrophilicity Index. Chem. Rev., 111(2), PR43-PR75..
[55] P.K. Chattaraj, S. Giri, S. Duley, Electrophilicity equalization principle, J. Phys. Chem. Lett. 1 (2010) 1064–1067.
[56] R.G. Parr, R.G. Pearson, Absolute hardness: companion parameter to absolute electronegativity, J. Am. Chem. Soc. 105 (1983) 7512–7516.
[57] https://www.researchgate.net/publication/258252733_Molecular_orbital_studies_hardness_chemical_potential_and_electrophilicity_vibrational_investigation_and_theoretical_NBO_analysis_of_4-4_'-1H-124-triazol-1-yl_methylene_dibenzonitrile _based_on_abiniti. [Accessed: 31-Mar-2019].
[58] R.G. Parr, R.A. Donnelly, M. Levy, W.E. Palke, Electronegativity: the density functional viewpoint, J. Chem. Phys. 68 (1978) 3801–3807.
[59] P. Politzer, D.G Truhlar, Chemical applications of atomic and molecular electrostatic potentials: reactivity, structure, scattering, and energetics of organic, inorganic, and biological systems, Springer Science & Business Media, 2013.
[60] R. Parthasarathi, J. Padmanabhan, M. Elango, V. Subramanian, P.K. Chattaraj, Intermolecular reactivity through the generalized philicity concept, Chem. Phys. Lett. 394 (2004) 225–230.
[61] T. Koopmans, Über die Zuordnung von Wellenfunktionen und Eigenwerten zu den einzelnen elektronen eines Atoms, Physica 1 (1934) 104–113.
[62] https://pubs.acs.org/doi/10.1021/ja983494x. [Accessed: 08-Apr-2019]
[63] R. Medishetty, J.K. Zaręba, D. Mayer, M. Samoć, R.A. Fischer, Nonlinear optical properties, upconversion and lasing in metal–organic frameworks, Chem. Soc. Rev. 46 (2017) 4976–5004.
[64] K.B. Manjunatha, R. Rajarao, G. Umesh, B.R. Bhat, P. Poornesh, Optical nonlinearity, limiting and switching characteristics of novel ruthenium metal-organic complex, Opt. Mater. 72 (2017) 513–517.